Results in Physics 8 (2018) 160–168

Contents lists available at ScienceDirect

Results in Physics

journal homepage: www.journals.elsevier.com/results-in-physics

Characteristics of buoyancy force on stagnation point flow with magneto-nanoparticles and zero mass flux condition

Iftikhar Uddin [a,*], Muhammad Altaf Khan [b], Saif Ullah [c], Saeed Islam [a], Muhammad Israr [d], Fawad Hussain [e]

[a] Department of Mathematics, Abdul Wali Khan University Mardan, 23200, Pakistan
[b] Department of Mathematics, City University of Science and Information Technology, Peshawar, KP 25000, Pakistan
[c] Department of Mathematics, Government Collge University Lahore, 54000, Pakistan
[d] Department of Mathematics, University of Malakand, Chakdara, KP 23050, Pakistan
[e] Department of Mathematics, Shaheed Benazir Bhutto University, Dir (Upper), KP, Pakistan

ARTICLE INFO

Article history:
Received 20 July 2017
Received in revised form 15 October 2017
Accepted 18 October 2017
Available online 10 November 2017

Keywords:
Stagnation point
MHD
Nanoparticles
Zero mass flux condition

ABSTRACT

This attempt dedicated to the solution of buoyancy effect over a stretching sheet in existence of MHD stagnation point flow with convective boundary conditions. Thermophoresis and Brownian motion aspects are included. Incompressible fluid is electrically conducted in the presence of varying magnetic field. Boundary layer analysis is used to develop the mathematical formulation. Zero mass flux condition is considered at the boundary. Non-linear ordinary differential system of equations is constructed by means of proper transformations. Interval of convergence via numerical data and plots are developed. Characteristics of involved variables on the velocity, temperature and concentration distributions are sketched and discussed. Features of correlated parameters on C_f and Nu are examined by means of tables. It is found that buoyancy ratio and magnetic parameters increase and reduce the velocity field. Further opposite feature is noticed for higher values of thermophoresis and Brownian motion parameters on concentration distribution.

Introduction

Nanofluid convective heat transfer has become an area of attention in research during the last few years. The term nanofluid is used for liquid suspension which contain particles of less than 50 nm in diameter. Research studies have shown that the thermal conductivity of the base liquid is increased to 50% (with a remarkable effect on the coefficient of the convective heat transfer) even with less than 5% volumetric fraction of nanoparticles. Boungiorno [1] discussed various theories which explain the characteristics of enhancement in heat transfer of nanoliquids. He also pointed out that the coefficients of high heat transfer in nanoliquids cannot be explored with satisfaction by the phenomena of thermal dispersion or increment in the intensity of turbulence that is enhanced by the existence of the nanoparticles or its rotation. Moreover, for convective transport in nanofluids, he has developed an analytical model taking into consideration thermophoresis and Brownian motion. Kuznetsov and Nield [2] have used Bounrgiorno's model in their study of natural convective naofluid flow on a vertical plate. Four parameters, namely the Brownian motion number, the buoyancy-ratio number, the thermophoresis number and the Lewis number (which govern the transport process) have been identified in their similarity analysis. Later these two researchers extended this research to a saturated porous medium of nanofluid [3]. Various authors have attempted in the same direction. Few of them are quoted in the Refs. [4–23]. The nanofluid flow at stagnation point and the process of heat transfer in the fluid and stretching surface is a significant problem of research. The problem is related to manufacturing goods and engineering problems as cooling of nuclear reactors during emergency shutdown, starching wire and plastic sheets and many more. When magnetic field is utilized to the fluid then the bounder layer flows of an electric conducted fluid on a stretching surface have increased the importance as research area and got attention of the researchers. The research in the area has wide applications. It is utilized in modern metal industry. Some studies related to MHD can be consulted via [24–29].

Flow on a stretching/shrinking surface can be utilized in many industrial firms like production of papers, drawing a wire glass fiber,to extract plastic sheets and in extracting plastic films. Crane [30] was the pioneer who started research on boundary layer flow on stretching/ shrinking sheet. Therefore there is much work on many aspects of the field, flow and heat transfer problems regard-

* Corresponding author.
E-mail address: iftikhar.8878@gmail.com (I. Uddin).

https://doi.org/10.1016/j.rinp.2017.10.038
2211-3797/© 2017 Published by Elsevier B.V.

ing stretching surface [31–38]. Mahapatra and Gupta [39] researched upon magnetohydrodynamic (MHD) heat transfer and stagnation point flow on a stretching surface. However Vijravalue [40] worked on the area of two dimensional (2D) flow produced via a non linear stretching surface. In the work it was supposed that sheet's velocity satisfy the power law distribution. Furthermore Cortell [42] researched on thermal radiation and viscous dissipation in the field. Hayat et al. [41] used Pade approximation and modified adomian decomposition techniques on magnetohydrodynamics (MHD) flow over a nonlinear stretching sheet. Rana and Bhargavargava [43] researched on the properties of the heat transfer and the flow of nanofluid because of non linear stretching sheet. Mukhopadhyay [44] explored the boundary layer flow on a permeable nonlinear stretching/shrinking sheet using partial slip condition. Mabood et al. [45] numerically analyzed the heat transfer and MHD flow of nanoliquid past a surface stretched nonlinearly. The axisymmetric nanofluid flow on a non linear stretching surface is worked out by Mustafa et al. [46]. They gave the the numerical and analytical solutions of the problems. Rashidi et al. [47] researched on the heat transfer and Darcy-Forchheimer flow around an hindrance of magnetic field effects. T. Hayat et al. [48] worked out magnetohydrodynamics 3D flow of second grade nanoliquid.

The study in hand is to explore the nanofluid flow on a stretching/shrinking surface under the effects of variable magnetic field, stagnation point, buoyancy force and convective heating. Novel surface condition known as zero mass flux condition is accounted. Mathematical formulations are access through boundary layer approach. Governing nonlinear system is solved via homotopic analysis technique [49–56]. Convergence is verified for the derived solutions. Graphs and tables are displayed to describe the physical significance of involved parameters.

Mathematical model of the problem

We begin our analysis by considering two-dimensional electrically conducting nanofluid flow in the region of stagnation point. Cartesian system is chosen in such a manner that x-axis is taken in the direction along which sheet is stretched and y-axis is perpendicular to it. A variable magnetic field $B = B_0(x)$ is applied transverse to the sheet. Assumption of small magnetic Reynolds number leads to ignore the induced field. Zero mass flux condition is addressed at the surface. The surface temperature is due to convective heating phenomena, which is attributed by coefficient of heat transport h_f and liquid temperature T_f. The combine effects of convective heating, buoyancy force, thermophoresis and Brownian motion are incorporated. The governing boundary layer expressions of the present flow analysis are [57,58] (Fig. 1):

$$\frac{\partial u}{\partial x} + \frac{\partial v}{\partial y} = 0, \tag{1}$$

$$u\frac{\partial u}{\partial x} + v\frac{\partial u}{\partial y} = U_\infty\frac{\partial U_\infty}{\partial x} + \frac{\mu_f}{\rho_f}\frac{\partial^2 u}{\partial y^2} - \frac{\sigma B^2(x)(u-U_\infty)}{\rho_f} + \frac{1}{\rho_f}\left[(1-\phi_\infty)\rho_{f_\infty}\beta g(T-T_\infty) + \left(\rho_p - \rho_\infty\right)g(\phi-\phi_\infty)\right], \tag{2}$$

$$u\frac{\partial T}{\partial x} + v\frac{\partial T}{\partial y} = \alpha_f\frac{\partial^2 T}{\partial y^2} + \frac{(\rho c)_p}{(\rho c)_f}\left[\frac{\partial C}{\partial y}\frac{\partial T}{\partial y} + \left(\frac{D_T}{T_\infty}\right)\left(\frac{\partial T}{\partial y}\right)^2\right], \tag{3}$$

$$u\frac{\partial C}{\partial x} + v\frac{\partial C}{\partial y} = D_B\frac{\partial^2 C}{\partial y^2} + \left(\frac{D_T}{T_\infty}\right)\left(\frac{\partial^2 T}{\partial y^2}\right), \tag{4}$$

with:

$$y = 0, \quad u = ax, \quad v = 0, \quad -k\frac{\partial T}{\partial y} = h_f(x)\left(T_f - T\right), \quad D_B\frac{\partial C}{\partial y} + \frac{D_T}{T_\infty}\frac{\partial T}{\partial y} = 0, \tag{5}$$

$$y \to \infty, \quad u \to U_\infty(x), \quad T \to T_\infty, \quad C \to C_\infty \tag{6}$$

Here (u, v) the respective velocities along (x, y) directions respectively. v is the kinematic viscosity, μ_f is the dynamic viscosity, ρ_f is the density of base fluid, ρ_p nanoparticles mass density, β the coefficient of thermal expansion, g the gravitational acceleration, σ is the electrical conductivity, $U_\infty = \frac{\alpha_f\sqrt{Ra_x}}{x}$ the external velocity, $Ra_x = \frac{(1-C_\infty)\beta g(T_f-T_\infty)x^3}{v\alpha_f}$ the local Rayleigh number, T the temperature, $\alpha_f = \frac{k}{(\rho c)_f}$ the thermal diffusivity of base fluid, k the thermal conductivity of the fluid, $(\rho c)_f$ the heat capacity of liquid, $(\rho c)_p$ the nanoparticles heat capacity, D_B the coefficient of Brownian diffusion, C the nanoparticles concentration, D_T the coefficient of thermophoretic diffusion, T_∞ and C_∞ denotes ambient temperature and nanoparticles concentration. The stream function $\psi(x, y)$ is expressed as follows

$$u = \frac{\partial\psi}{\partial y}, \quad v = -\frac{\partial\psi}{\partial x}, \tag{7}$$

while the dimensionless and similarity variables are introduce as [46,47]

$$\eta = \frac{y}{x}Ra_x^{\frac{1}{4}}, \quad \psi = \alpha_f Ra_x^{\frac{1}{4}}f(\eta), \quad \theta(\eta) = \frac{T-T_\infty}{T_f-T_\infty}, \quad \phi = \frac{C-C_\infty}{C_\infty}. \tag{8}$$

By using the stream function and similarity transformation, Eq. (1) is identically satisfied and Eqs. (2)–(6) yield [57]

$$f''' - M(f'-1) + \frac{1}{4\,\mathrm{Pr}}\left(3ff'' - 2f'^2 + 2\right) + \theta - Nr\phi = 0, \tag{9}$$

$$\theta'' + \frac{3}{4}f\theta' + N_b\phi'\theta' + N_t\theta'^2 = 0, \tag{10}$$

$$\phi'' + \frac{N_t}{N_b}\theta'' + \frac{3}{4}Lef\phi' = 0, \tag{11}$$

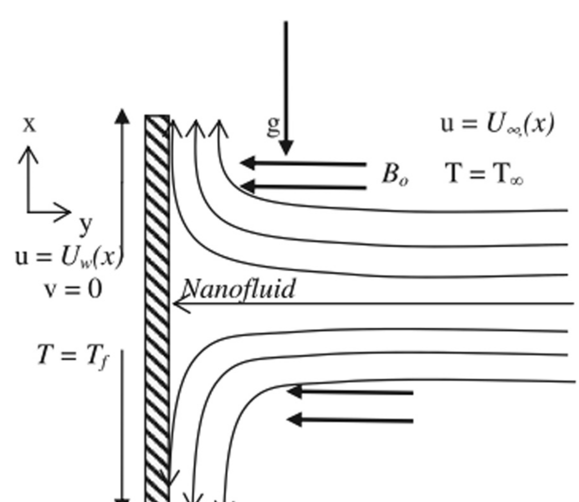

Fig. 1. Geometry discribing the problem.

$$f(0)=0,\quad f'(0)=\lambda,\quad \theta'(0)=-\gamma[1-\theta(0)],$$
$$\phi'(0)+\frac{Nt}{Nb}\theta'(0)=0 \quad \text{at} \quad \eta=0, \tag{12}$$

$$f'(\infty)=1,\quad \theta'(\infty)=0,\quad \phi(\infty)=0 \quad \text{as} \quad \eta\to\infty, \tag{13}$$

where M stands for magnetic parameter, N_t for thermophoritic variable, Nr for buoyancy-ratio parameter, N_b for diffusion variable, Pr for Prandtl, Le for Lewis number, λ and γ for stretching/shrinking parameter and Biot number respectively. These parameters and dimensionless numbers are defined as follows:

$$\left.\begin{array}{l} Nr=\frac{(\rho_p-\rho_f)(C_w-C_\infty)}{\rho_f\beta(1-C_w)(T_f-T_\infty)},\quad N_b=\frac{\tau D_B(C_w-C_\infty)}{\alpha_f},\\ \Pr=\frac{\upsilon}{\alpha},\quad Le=\frac{\alpha_f}{D_B},\quad M=\sigma B_0^2(x)\frac{\sqrt{\frac{x}{C_1}}}{\mu_f},\\ N_t=\frac{(\rho c)_p D_T(T_f-T_\infty)}{(\rho c)_f\upsilon T_\infty},\quad \gamma=\frac{h_f x^{\frac{1}{4}}}{k}\left[\frac{\upsilon\alpha_f}{g\beta(1-C_w)(T_f-T_\infty)}\right]^{\frac{1}{4}},\\ C_1=\frac{g\beta(1-C_w)(T_f-T_\infty)}{\upsilon\alpha_f},\quad \lambda=\frac{ax^2}{\alpha_f\sqrt{Ra_x}}. \end{array}\right\} \tag{14}$$

Skin friction C_f and local Nusselt number Nu_r are [57]:

$$C_f=\frac{\tau_w x^2}{\alpha_f\mu_f Ra_x^{\frac{3}{4}}},\quad Nu_r=\frac{q_w x}{k(T_w-T_\infty)}, \tag{15}$$

where τ_w and q_w are the wall shear stresses and heat flux. In non-dimensional form we have:

$$C_f=f''(0),\quad Nu_r=\mathrm{Re}_x^{-\frac{1}{2}}Nu=-\theta'(0). \tag{16}$$

The homotopic solutions

Liao [49] in 1992 proposed homotopy analysis method to solve the highly nonlinear equations. It is a continuous deformation or change of a function or equation. Moreover, it is independent of small or large physical parameters. It has many advantages when compared to other methods i.e. (*i*) it is independent of small or large parameters (*ii*) it confirms the convergence of series solution (*iii*) it provides great freedom to choose the base function and linear operator. Such flexibility and freedom assist in solving the highly nonlinear problems. The initial estimations (f_0,θ_0,ϕ_0) and operators $(\bar{\mathcal{L}}_f,\bar{\mathcal{L}}_\theta,\bar{\mathcal{L}}_\phi)$ are:

$$f_0(\eta)=1-e^{-\eta},\quad \theta_0(\eta)=\frac{\gamma}{1+\gamma}e^{-\eta},\quad \phi_0(\eta)=e^{-\eta}, \tag{17}$$

$$\bar{\mathcal{L}}_f=f'''-f',\quad \bar{\mathcal{L}}_\theta=\theta''-\theta,\quad \bar{\mathcal{L}}_\phi=\phi''-\phi, \tag{18}$$

with

$$\bar{\mathcal{L}}_f[\tilde{c}_1+\tilde{c}_2e^{\eta}+\tilde{c}_3e^{-\eta}]=0,\quad \bar{\mathcal{L}}_\theta[\tilde{c}_4e^{\eta}+\tilde{c}_5e^{-\eta}]=0,$$
$$\bar{\mathcal{L}}_\phi[\tilde{c}_6e^{\eta}+\tilde{c}_7e^{-\eta}]=0, \tag{19}$$

in which $\tilde{c}_i$ $(i=1-7)$ represents the arbitrary constants.

The zeroth order problems of this model

$$(1-\check{\text{Þ}})\bar{\mathcal{L}}_f\left[\hat{f}(\eta,\check{\text{Þ}})-f_0(\eta)\right]=\check{\text{Þ}}\hbar_f\mathcal{N}_f[\hat{f}(\eta,\check{\text{Þ}}),\hat{\theta}(\eta,\check{\text{Þ}}),\hat{\phi}(\eta,\check{\text{Þ}})], \tag{20}$$

$$(1-\check{\text{Þ}})\bar{\mathcal{L}}_\theta\left[\hat{\theta}(\eta,\check{\text{Þ}})-\theta_0(\eta)\right]=\check{\text{Þ}}\hbar_\theta\mathcal{N}_\theta[\hat{f}(\eta,\check{\text{Þ}}),\hat{\theta}(\eta,\check{\text{Þ}}),\hat{\phi}(\eta,\check{\text{Þ}})], \tag{21}$$

$$(1-\check{\text{Þ}})\bar{\mathcal{L}}_\phi\left[\hat{\phi}(\eta,\check{\text{Þ}})-\phi_0(\eta)\right]=\check{\text{Þ}}\hbar_\phi\mathcal{N}_\phi[\hat{f}(\eta,\check{\text{Þ}}),\hat{\theta}(\eta,\check{\text{Þ}}),\hat{\phi}(\eta,\check{\text{Þ}})], \tag{22}$$

$$\hat{f}(0,\check{\text{Þ}})=0,\quad \hat{f}'(0,\check{\text{Þ}})=\lambda,\quad \hat{f}'(\infty,\check{\text{Þ}})=0,\quad \hat{\theta}'(0,\check{\text{Þ}})=-\gamma(1-\hat{\theta}(0,\check{\text{Þ}})), \tag{23}$$

$$\hat{\theta}(\infty,\check{\text{Þ}})=0,\quad N_b\hat{\phi}'(0,\check{\text{Þ}})+N_t\hat{\theta}'(0,\check{\text{Þ}})=0,\quad \hat{\phi}(\infty,\check{\text{Þ}})=0, \tag{24}$$

$$\mathcal{N}_f\left[\hat{f}(\eta;\check{\text{Þ}})\right]=\frac{\partial^3\hat{f}}{\partial\eta^3}+\hat{f}\frac{\partial^2\hat{f}}{\partial\eta^2}-2\left(\frac{\partial\hat{f}}{\partial\eta}+\frac{\partial\hat{g}}{\partial\eta}\right)\frac{\partial\hat{f}}{\partial\eta}-\left(\frac{\partial\hat{f}}{\partial\eta}\right)^2 \tag{25}$$

$$\mathcal{N}_\theta\left[\hat{\theta}(\eta,\check{\text{Þ}}),\hat{\phi}(\eta,\check{\text{Þ}}),\hat{f}(\eta;\check{\text{Þ}})\right]=\frac{\partial^2\hat{\theta}}{\partial\eta^2}+\frac{3}{4}\hat{f}\frac{\partial\hat{\theta}}{\partial\eta}+N_b\frac{\partial\hat{\theta}}{\partial\eta}\frac{\partial\hat{\phi}}{\partial\eta}+N_t\left(\frac{\partial\hat{\theta}}{\partial\eta}\right)^2, \tag{26}$$

$$\mathcal{N}_\phi[\hat{\phi}(\eta,\check{\text{Þ}}),\hat{\theta}(\eta,\check{\text{Þ}}),\hat{f}(\eta;\check{\text{Þ}})]=\frac{\partial^2\hat{\phi}}{\partial\eta^2}+\frac{3}{4}Le\hat{f}\frac{\partial\hat{\phi}}{\partial\eta}+\left(\frac{N_t}{N_b}\right)\frac{\partial^2\theta}{\partial\eta^2}. \tag{27}$$

Here $(\hbar_f,\hbar_\theta,\hbar_\phi)$ and $\check{\text{Þ}}\in[0,1]$ are auxiliary and embedding variables respectively, $\mathcal{N}_f,\mathcal{N}_\theta$ and $\mathcal{N}_\phi$ are the nonlinear operators. For $\check{\text{Þ}}=0$ and $\check{\text{Þ}}=1$ we get

$$\hat{f}(\eta;0)=f_0(\eta),\hat{\theta}(\eta,0)=\theta_0(\eta),\hat{\phi}(\eta,0)=\phi_0(\eta), \tag{28}$$

$$\hat{f}(\eta;1)=f(\eta),\hat{\theta}(\eta,1)=\theta(\eta),\hat{\phi}(\eta,1)=\phi(\eta). \tag{29}$$

When $\check{\text{Þ}}$ approaches from 0 to 1 then $\hat{f}(\eta;\check{\text{Þ}})$, $\hat{\theta}(\eta,\check{\text{Þ}})$ and $\hat{\phi}(\eta,\check{\text{Þ}})$ approaches from the initial guesses $(f_0(\eta),\theta_0(\eta),\phi_0(\eta))$ to the final expressions $(f(\eta),\theta(\eta),\phi(\eta))$ respectively.

$$\hat{f}(\eta;\check{\text{Þ}})=f_0(\eta)+\sum_{m=1}^{\infty}f_m(\eta)\check{\text{Þ}}^m,\quad f_m(\eta)=\frac{1}{m!}\frac{\partial^m\hat{f}(\eta,\check{\text{Þ}})}{\partial\check{\text{Þ}}^m}\bigg|_{\check{\text{Þ}}=0}, \tag{30}$$

$$\hat{\theta}(\eta,\check{\text{Þ}})=\theta_0(\eta)+\sum_{m=1}^{\infty}\theta_m(\eta)\check{\text{Þ}}^m,\quad \theta_m(\eta)=\frac{1}{m!}\frac{\partial^m\hat{\theta}(\eta,\check{\text{Þ}})}{\partial\check{\text{Þ}}^m}\bigg|_{\check{\text{Þ}}=0}, \tag{31}$$

$$\hat{\phi}(\eta,\check{\text{Þ}})=\phi_0(\eta)+\sum_{m=1}^{\infty}\phi_m(\eta)\check{\text{Þ}}^m,\quad \phi_m(\eta)=\frac{1}{m!}\frac{\partial^m\hat{\phi}(\eta,\check{\text{Þ}})}{\partial}\check{\text{Þ}}^m\bigg|_{\check{\text{Þ}}=0}. \tag{32}$$

Here $\hbar_f,\hbar_\theta$ and $\hbar_\phi$ are selected in such a way that the series (30)–(32) converge at $\check{\text{Þ}}=1$, we have

$$f(\eta)=f_0(\eta)+\sum_{m=1}^{\infty}f_m(\eta), \tag{33}$$

$$\theta(\eta)=\theta_0(\eta)+\sum_{m=1}^{\infty}\theta_m(\eta), \tag{34}$$

$$\phi(\eta)=\phi_0(\eta)+\sum_{m=1}^{\infty}\phi_m(\eta). \tag{35}$$

The mth order deformations are defined for this model by:

$$\bar{\mathcal{L}}_f\left[f_m(\eta)-\chi_m f_{m-1}(\eta)\right]=\hbar_f\check{\mathcal{R}}_f^m(\eta), \tag{36}$$

$$\bar{\mathcal{L}}_\theta\left[\theta_m(\eta)-\chi_m\theta_{m-1}(\eta)\right]=\hbar_\theta\check{\mathcal{R}}_\theta^m(\eta), \tag{37}$$

$$\bar{\mathcal{L}}_\phi\left[\phi_m(\eta)-\chi_m\phi_{m-1}(\eta)\right]=\hbar_\phi\check{\mathcal{R}}_\phi^m(\eta), \tag{38}$$

$$\left.\begin{array}{l} f_m(0)=f'_m(0)=f'_m(\infty)=0,\quad \theta'_m(0)-\gamma\theta_m(0)=0,\\ \theta_m(\infty)=0,\quad N_b\phi'_m(0)+N_t\theta'_m(0)=0,\quad \phi_m(\infty)=0. \end{array}\right\} \tag{39}$$

$$\check{\mathcal{R}}_f^m(\eta)=f'''_{m-1}(\eta)-Mf'_{m-1}(\eta)+M+\frac{3}{4\Pr}\sum_{k=0}^{m-1}f_{m-1-k}f''_k$$
$$-\frac{1}{2\Pr}\sum_{k=0}^{m-1}f'_{m-1-k}f'_k+\frac{1}{2\Pr}+\theta_{m-1}-Nr\phi, \tag{40}$$

$$\check{\mathcal{R}}_{\theta}^{m}(\eta) = \theta''_{m-1}(\eta) + \frac{3}{4}\sum_{k=0}^{m-1} f_{m-1-k}\theta'_k + N_b \sum_{k=0}^{m-1}\phi'_{m-1-k}\theta'_k + N_t \sum_{k=0}^{m-1}\theta'_{m-1-k}\theta'_k, \quad (41)$$

$$\check{\mathcal{R}}_{\phi}^{m}(\eta) = \phi''_{m-1}(\eta) + \frac{3}{4}Le\sum_{k=0}^{m-1}(f_{m-1-k}\phi'_k) + \frac{N_t}{N_b}\theta''_{m-1}(\eta), \quad (42)$$

$$\chi_m = \begin{cases} 0, & m \leqslant 1, \\ 1, & m > 1. \end{cases} \quad (43)$$

The mth-order deformation problem have the solution in terms of special expressions $f_m^*(\eta), \theta_m^*(\eta)$ and $\phi_m^*(\eta)$ are designated as follows:

$$f_m(\eta) = f_m^*(\eta) + \tilde{c}_1 + \tilde{c}_2 e^{\eta} + \tilde{c}_3 e^{-\eta}, \quad (44)$$

$$\theta_m(\eta) = \theta_m^*(\eta) + \tilde{c}_4 e^{\eta} + \tilde{c}_5 e^{-\eta}, \quad (45)$$

$$\phi_m(\eta) = \phi_m^*(\eta) + \tilde{c}_6 e^{\eta} + \tilde{c}_7 e^{-\eta}, \quad (46)$$

where $\tilde{c}_i$ $(i = 1–7)$ are constants, subject to (39) express as follows:

$$\left.\begin{array}{l} \tilde{c}_2 = \tilde{c}_4 = \tilde{c}_6 = 0, \quad \tilde{c}_3 = \left.\frac{\partial f_m^*(\eta)}{\partial \eta}\right|_{\eta=0}, \quad \tilde{c}_1 = -\tilde{c}_3 - f_m^*(0), \\ \tilde{c}_5 = \frac{1}{1+\gamma}\left(\left.\frac{\partial \theta_m^*(\eta)}{\partial \eta}\right|_{\eta=0} - \gamma\theta_m^*(0)\right), \quad \tilde{c}_7 = \left.\frac{\partial \phi_m^*(\eta)}{\partial \eta}\right|_{\eta=0} + \frac{N_t}{N_b}\left(-\tilde{c}_5 + \left.\frac{\partial \theta_m^*(\eta)}{\partial \eta}\right|_{\eta=0}\right). \end{array}\right\} \quad (47)$$

The convergence of homotopic solutions

The $(\hbar_f, \hbar_\theta, \hbar_\phi)$ corresponds to auxiliary parameters for $(f(\eta), \theta(\eta), \phi(\eta))$ respectively. These auxiliary parameters play key role to control and adjust the convergence of resultant series solutions. To attain the appropriate values of these parameters, we plotted the $\hbar$-curves for $f''(0), \theta'(0)$ and $\phi'(0)$ at 15th order of approximations see (Figs. 2 and 3). It is noticed that the acceptable ranges of $(\hbar_f, \hbar_\theta$ and $\hbar_\phi)$ are $-0.8 \leqslant \hbar_f \leqslant -0.1, -1.0 \leqslant \hbar_\theta \leqslant -0.0001$ and $-1.0 \leqslant \hbar_\phi \leqslant -0.02$. Table 1 shows the convergence of series solutions for the functions $(f(\eta), \theta(\eta), \phi(\eta))$ by adjusting particular value of auxiliary parameters. It is noticeable that 15th order of estimations are enough for the convergence of $f(\eta), \theta(\eta)$ and $\phi(\eta)$.

Discussion

This portion aims to investigate the characteristics of some influential variables like magnetic parameter (M), buoyancy-ratio parameter (Nr), Prandtl number (Pr), Thermophoresis variable (N_t), Brownian diffusion variable (N_b), stretching/shrinking parameter (λ) and Lewis number (Le) on the velocity $f'(\eta)$, temperature $\theta(\eta)$ and nanoparticles concentration $\phi(\eta)$. For such purpose Figs. 4–15 are prepared to illustrate the results of these parameters. We have constructed Fig. 4 for the velocity profile $f'(\eta)$ for various values of Prandtl number. Here we noticed from this Fig. that increment in Pr cause a reduction in velocity profile. In fact the fluid velocity enhances with the increase in Pr. That is why $f'(\eta)$ diminishes. Fig. 5 represents the impact of M on the $f'(\eta)$. Here larger values of M reduce the fluid velocity. It is because of the fact that the applications of magnetic field utilized in normal direction creates Lorentz force (resistive type force). Such force reduce velocity field. The characteristics of shrinking/stretching parameter λ is represented in Fig. 6. Here the $f'(\eta)$ at the surface is noted to be enhances and diminishes with stretching and shrinking respectively. In fact the flow is accelerated with greater suction (less negative velocity values arise) and this decreases momentum boundary layer thickness. As a result, suction can be used effectively for controlling the momentum boundary layer growth/decay by using stretching/shrinking sheets respectively. Fig. 7 is prepared to check the characteristics of the Nr on the $f'(\eta)$. It is lucid that the $f'(\eta)$ reduces when we pronounce the Nr. Physically concentration

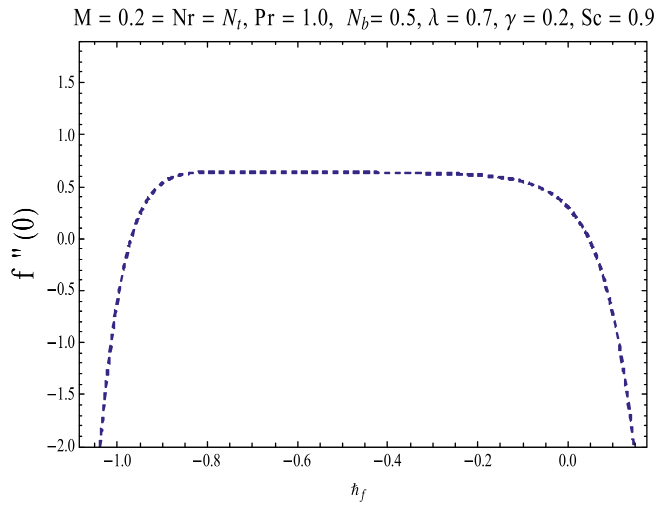

Fig. 2. The $\hbar$-curves for $f(\eta)$.

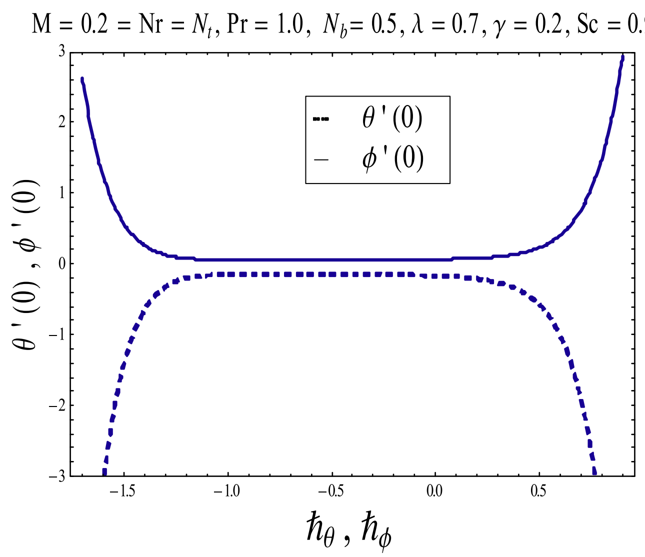

Fig. 3. The $\hbar$-curves for $\theta(\eta)$ and $\phi(\eta)$.

Table 1
Solutions convergence when $M = Nr = N_t = \gamma = 0.2$, $\Pr = 1.0$, $N_b = 0.5$, $\lambda = 0.7$, $Le = 0.9$.

Order of approximations	$f''(0)$	$-\theta'(0)$	$\phi'(0)$
1	0.5100	0.1618	0.0647
5	0.6241	0.1542	0.0617
10	0.6338	0.1530	0.0612
11	0.6341	0.1530	0.0612
12	0.6342	0.1529	0.0612
13	0.6343	0.1529	0.0612
14	0.6344	0.1529	0.0612
15	0.6345	0.1529	0.0612
16	0.6342	0.1529	0.0612
17	0.6342	0.1529	0.0611

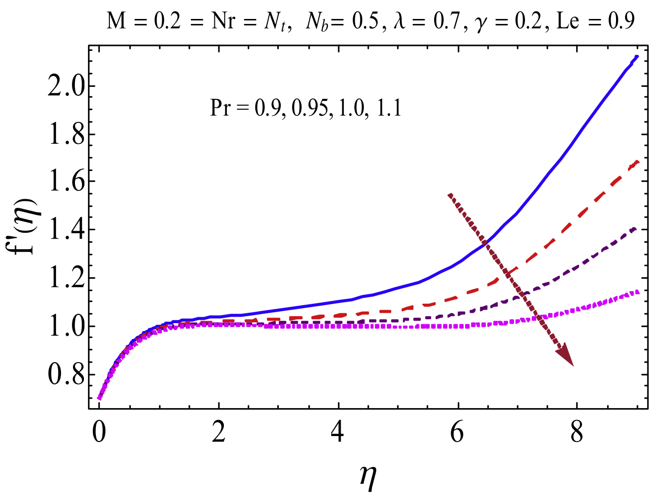

Fig. 4. Behaviour of $f'(\eta)$ via Pr.

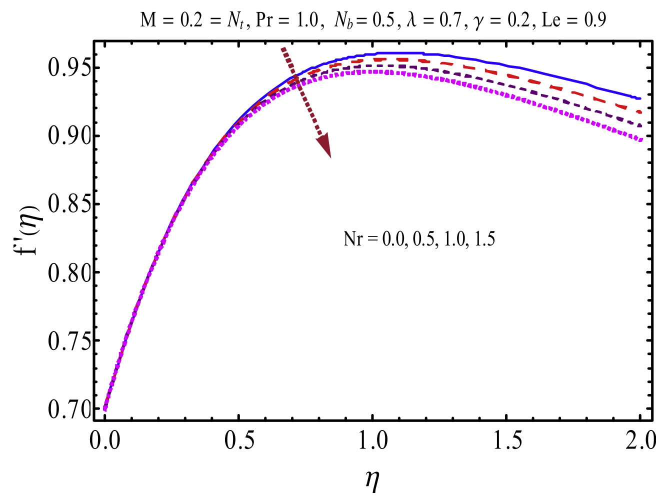

Fig. 7. Behavior of $f'(\eta)$ via Nr.

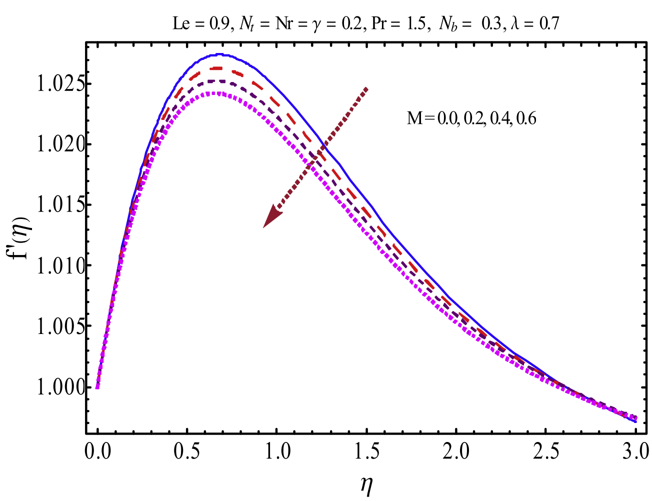

Fig. 5. Behaviour of $f'(\eta)$ via M.

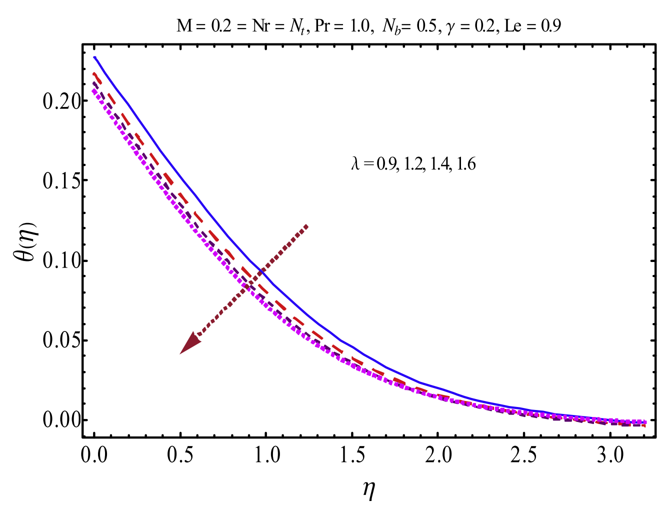

Fig. 8. Behavior of $\theta(\eta)$ via λ.

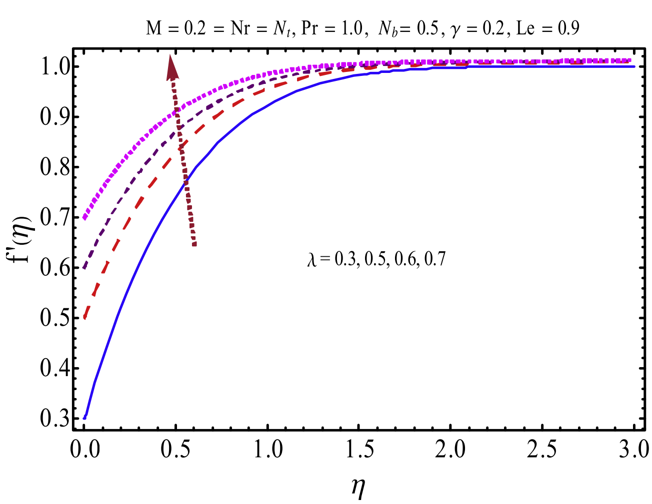

Fig. 6. Behaviour of $f'(\eta)$ via λ.

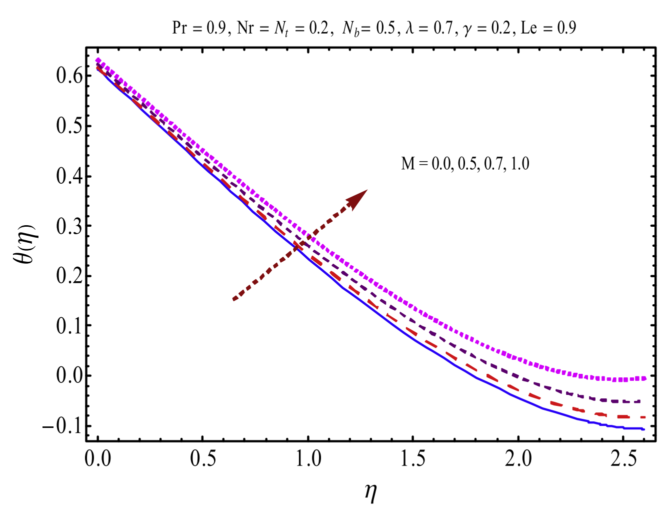

Fig. 9. Behavior of $\theta(\eta)$ via M.

buoyancy force increases via larger Nr which yields higher velocity. Fig. 8 depicts changes temperature field $\theta(\eta)$ for increasing values of stretching/shrinking parameter λ. Here larger values of λ gives reduction in temperature field. Fig. 9 is plotted for the temperature profile using different values of magnetic parameter M, while other parameters are fixed. Here larger values of M enhance the temper-

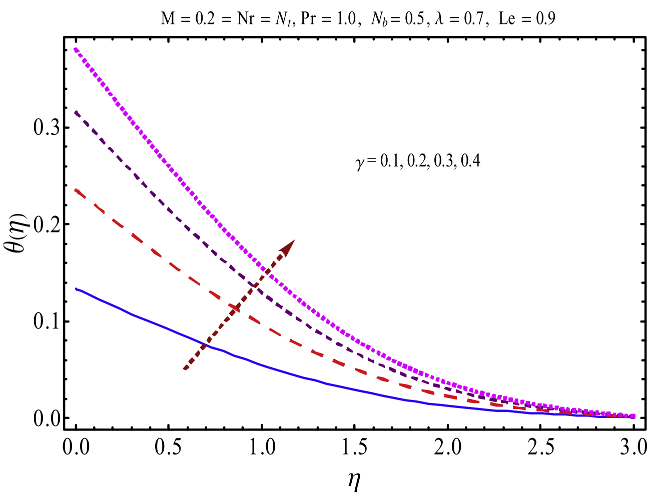

Fig. 10. Behavior of $\theta(\eta)$ via γ.

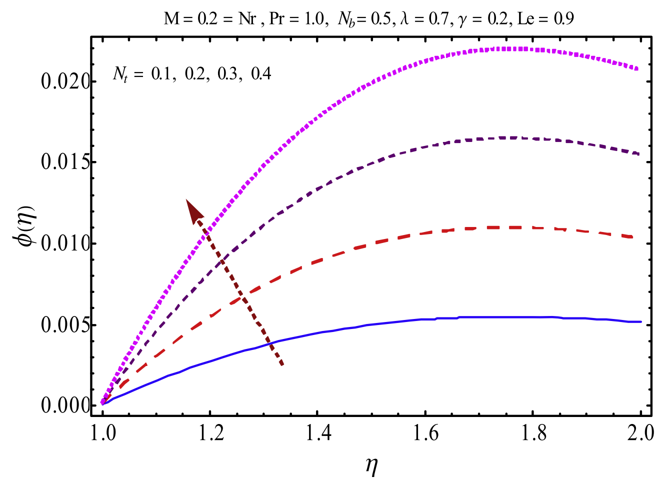

Fig. 13. Behavior of $\phi(\eta)$ via N_t.

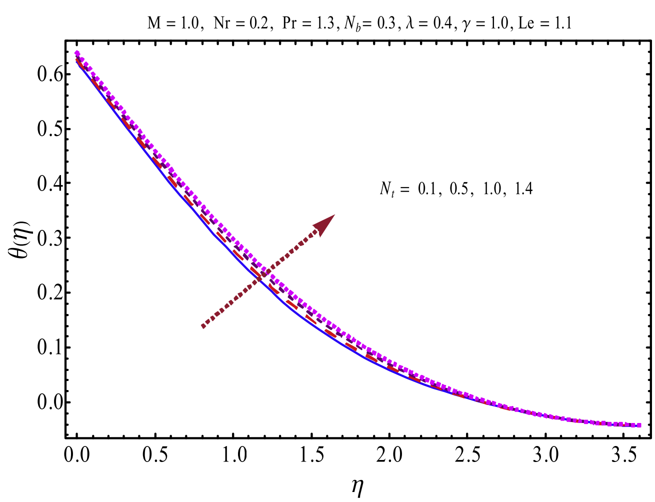

Fig. 11. Behavior of $\theta(\eta)$ via N_t.

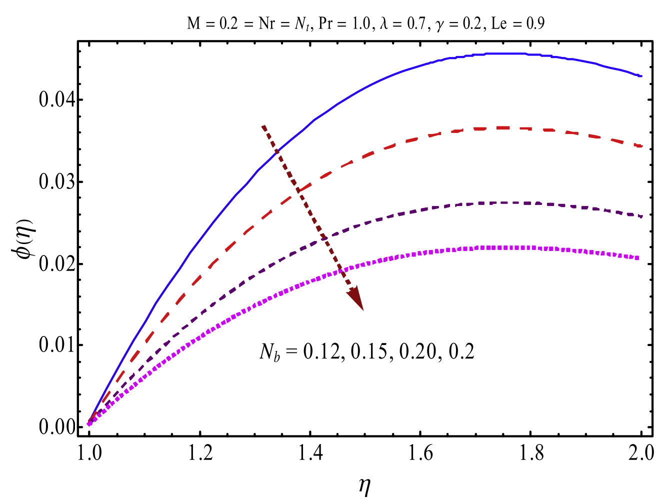

Fig. 14. Behavior of $\phi(\eta)$ via N_b.

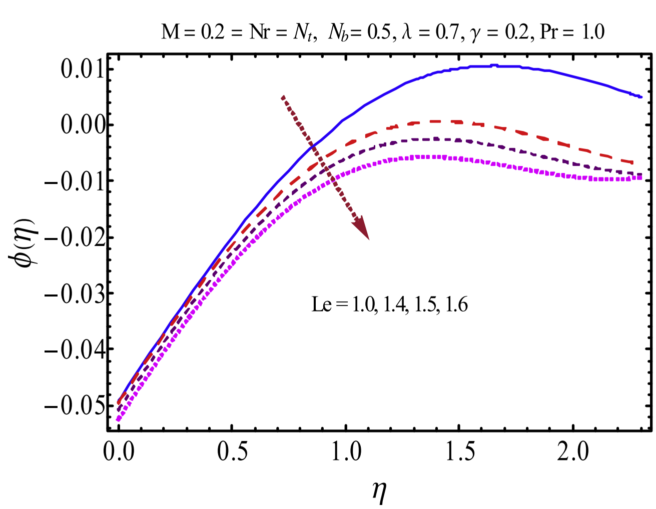

Fig. 12. Behavior of $\phi(\eta)$ via *Le*.

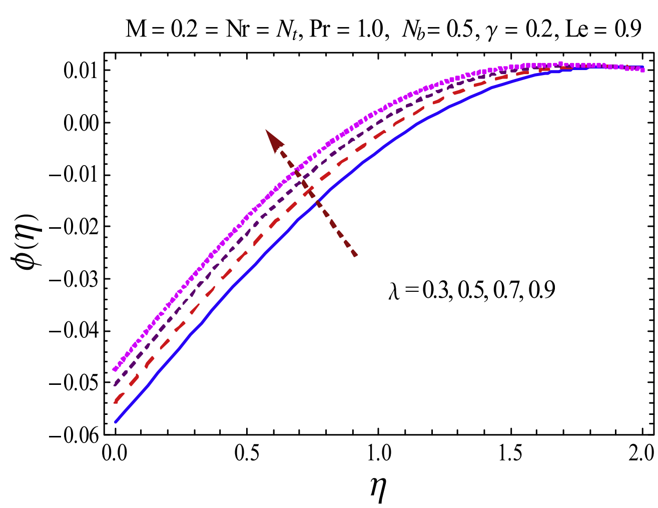

Fig. 15. Behavior of $\phi(\eta)$ via λ.

ature field. This rise in temperature is due to heat generated by resistive force caused by magnetic field. Further, the graph shows that the thickness regarding the thermal boundary layer usually enhances for higher M. Fig. 10 declares the significance of Biot number γ on $\theta(\eta)$. This figure points out that an increment in γ brings an enhancement in $\theta(\eta)$. Physically the involvement of lar-

Table 2
Numerical data of skin friction for different values of physical variables.

γ	Le	λ	M	N_b	N_t	Nr	Pr	C_f
0.0	0.9	0.7	0.2	0.5	0.2	0.2	1.0	0.0.5381
0.2								0.6342
0.4								0.6930
0.2	0.7	0.7	0.2	0.5	0.2	0.2	1.0	0.6347
	0.8							0.6343
	0.9							0.6342
0.2	0.9	0.3	0.2	0.5	0.2	0.2	1.0	1.267
		0.5						0.9657
		0.7						0.6342
0.2	0.9	0.7	0.0	0.5	0.2	0.2	1.0	0.6195
			0.3					0.6417
			0.6					0.6628
0.2	0.9	0.7	0.2	0.1	0.2	0.2	1.0	0.6448
				0.2				0.6381
				0.4				0.6351
0.2	0.9	0.7	0.2	0.5	0.1	0.2	1.0	0.6327
					0.3			0.6357
					0.5			0.6387
0.2	0.9	0.7	0.2	0.5	0.2	0.0	1.0	0.6318
						0.2		0.6342
						0.4		0.6368
0.2	0.9	0.7	0.2	0.5	0.2	0.2	1.1	0.6136
							1.2	0.5957
							1.3	0.5801

Table 3
Computations for surface heat transfer rate at distinct physical variables.

γ	Le	λ	M	Nb	Nt	Nr	Pr	$Ra_x^{\frac{1}{2}}Nu_x$
0.1	0.9	0.7	0.2	0.5	0.2	0.2	1.0	0.08663
0.2								0.1529
0.4								0.2478
0.2	0.7	0.7	0.2	0.5	0.2	0.2	1.0	0.1529
	0.9							0.1529
	1.2							0.1529
0.2	0.9	0.2	0.2	0.5	0.2	0.2	1.0	0.1481
		0.4						0.1502
		0.6						0.1520
0.2	0.9	0.7	0.0	0.5	0.2	0.2	1.0	0.1529
			0.3					0.1529
			0.5					0.1530
0.2	0.9	0.7	0.2	0.1	0.2	0.2	1.0	0.1529
				0.2				0.1529
				0.4				0.1529
0.2	0.9	0.7	0.2	0.5	0.1	0.2	1.0	0.1530
					0.3			0.1528
					0.5			0.1527
0.2	0.9	0.7	0.2	0.5	0.2	0.0	1.0	0.1529
						0.3		0.1529
						0.6		0.1529
0.2	0.9	0.7	0.2	0.5	0.2	0.2	1.1	0.1531
							1.2	0.1530
							1.3	0.1529

ger heat transfer coefficient correspond to high temperature. It is found from Fig. 11 that the temperature field $\theta(\eta)$ has increasing characteristics when we increase the value of N_t. Thermophoresis is a phenomenon in small particles are pulled away from the hot surface to cold one. For larger thermophoresis parameters hot fluid particles move away from the surface and consequently the temperature profile increases. Impact of Le on $\phi(\eta)$ is explored in Fig. 12. It is revealed that both the concentration and similarly layer thickness reduce for greater values of Le. Physically there is inverse relation between Le and N_b. Higher Le results in weaker Brownian diffusion coefficient which consequently produces reduction in $\phi(\eta)$. Fig. 13 shows that the change in nanoparticles concentration $\phi(\eta)$ for various values of N_t. Here $\phi(\eta)$ enhances via N_t. Itillustrates that for larger thermophoresis parameter more particles are pushed far from the hot surface which results in the enhancement of concentration profile. Fig. 14 shows that larger N_b causes a weaker concentration $\phi(\eta)$. Larger N_b leads to an increase in the nanoparticles' motion and consequently the viscosity of nanofluid decreases. That is why the nanoparticles' concentration and its related boundary layer thickness reduces. Fig. 15

is plotted to see the behavior of stretching/shrinking parameter λ. Here nanoparticles concentration increases and the corresponding boundary layer get thicker when we increase λ. Table 1 is computed for distinct order of estimations of $-f''(0), -\theta'(0)$ and $\phi'(0)$ when $M = Nr = N_t = \gamma = 0.2, \Pr = 1.0, N_b = 0.5, \lambda = 0.7, Le = 0.9$ and $\hbar_f = \hbar_\theta = -0.5 = \hbar_\phi$. This table demonstrates that the values of $-f''(0), -\theta'(0)$ and $\phi'(0)$ converge at 16th order of deformations. Table 2 is developed to view the characteristics of various embedding variables on surface drag force. It is revealed that skin friction (C_f) is increased when we enhance Nr, M and Pr. Table 3 is prepared to compute the numerical data of Nusselt number for distinct values of emerging parameters. Here we see that Nusselt number is enhanced when we rise the values of N_t and Pr. Similarly the opposite behavior is seen for the Biot number γ.

Closing remarks

Features of buoyancy force on MHD flow of nanoliquid in the region of stagnation point flow subject to zero mass flux condition is studied. Main findings of present analysis are mentioned below:

- The velocity $f'(\eta)$ profile decreases by increasing values of the M and alternatively temperature $\theta(\eta)$ profile enhances.
- Velocity $f'(\eta)$ decreases with the increment in Nr.
- An enhancement in γ leads to stronger temperature field $\theta(\eta)$.
- Effects of λ on velocity $\theta(\eta)$ and $\phi(\eta)$ are similar.
- Higher N_t shows similar characteristics for $\theta(\eta)$ and $\phi(\eta)$.
- Surface drag force is higher for higher magnetic parameter M.
- Heat transfer rate at the sheet is uniform for N_b while it is lower for thermophoresis parameter N_t.

References

[1] Buongiorno J. Convective transport in nanofluids. J Heat Transfer 2006;128:240–50.
[2] Kuznetsov AV, Nield DA. Natural convective boundary-layer flow of a nanofluid past a vertical plate. Int J Therm Sci 2010;49:243–7.
[3] Nield DA, Kuznetsov AV. The Chenge Minkowycz problem for natural convective boundary-layer flow in a porous medium saturated by a nanofluid. Int J Heat Mass Transfer 2009;52:5792–5.
[4] Hayat T, Sajjad R, Alsaedi A, Muhammad T, Ellahi R. On squeezing flow of couple stress nanofluid between two parallel plates. Results Phys 2017;7:553–61.
[5] Rahman SU, Ellahi R, Nadeem S, Zaigham Zia QM. Simultaneous effects of nanoparticles and slip on Jeffrey fluid through tapered artery with mild stenosis. J Mol Liq 2016;218:484–93.
[6] Akbarzadeh M, Rashidi S, Bovand M, Ellahi R. A sensitivity analysis on thermal and pumping power for the flow of nanofluid inside a wavy channel. J Mol Liq 2016;220:1–13.
[7] Shirvan Kamel Milani, Mamourian Mojtaba, Mirzakhanlari Soroush, Ellahi R. Two phase simulation and sensitivity analysis of effective parameters on combined heat transfer and pressure drop in a solar heat exchanger filled with nanofluid by RSM. J Mol Liq 2016;220:888–901.
[8] Shehzad N, Zeeshan A, Ellahi R, Vafai K. Convective heat transfer of nanofluid in a wavy channel: Buongiorno's mathematical model. J Mol Liq 2016;222:446–55.
[9] Ellahi R, Zeeshan A, Hassan M. Particle shape effects on marangoni convection boundary layer flow of a nanofluid. Int J Numer Methods Heat Fluid Flow 2016;26(7):2160–74.
[10] Shirvan KM, Ellahi R, Mamourian M, Moghiman M. Effect of wavy surface characteristics on heat transfer in a wavy square cavity filled with nanofluid. Int J Heat Mass Transfer 2017;107:1110–8.
[11] Ellahi R, Tariq MH, Hassan M, Vafai K. On boundary layer magnetic flow of nano-Ferroliquid under the influence of low oscillating over stretchable rotating disk. J Mol Liq 2017;229:339–45.
[12] Shirvan KM, Mamourian M, Mirzakhanlari S, Ellahi R. Numerical investigation of heat exchanger effectiveness in a double pipe heat exchanger filled with nanofluid: a sensitivity analysis by response surface methodology. Power Technol 2017;313:99–111.
[13] Hayat T, Ijaz Khan M, Waqas M, Alsaedi A, Khan MI. Radiative flow of micropolar nanofluid accounting thermophoresis and Brownian moment. Int J Hydrogen Energy 2017;42:16821–33.
[14] Hayat T, Waqas M, Shehzad SA, Alsaedi A. A model of solar radiation and Joule heating in magnetohydrodynamic (MHD) convective flow of thixotropic nanofluid. J Mol Liq 2016;215:704–10.
[15] Waqas M, Khan MI, Hayat T, Alsaedi A. Numerical simulation for magneto Carreau nanofluid model with thermal radiation: a revised model. Comput Methods Appl Mech Eng 2017;324:640–53.
[16] Hayat T, Khan MI, Waqas M, Alsaedi A, Farooq M. Numerical simulation for melting heat transfer and radiation effects in stagnation point flow of carbon–water nanofluid. Comput Methods Appl Mech Eng 2017;315:1011–24.
[17] Hayat T, Waqas M, Khan MI, Alsaedi A. Analysis of thixotropic nanomaterial in a doubly stratified medium considering magnetic field effects. Int J Heat Mass Transfer 2016;102:1123–9.
[18] Ijaz Khan M, Waqas M, Hayat T, Khan MI, Alsaedi A. Behavior of stratification phenomenon in flow of Maxwell nanomaterial with motile gyrotactic microorganisms in the presence of magnetic field. Int J Mech Sci 2017;131–132:426–34.
[19] Hayat T, Bashir G, Waqas M, Alsaedi A. MHD 2D flow of Williamson nanofluid over a nonlinear variable thicked surface with melting heat transfer. J Mol Liq 2016;223:836–44.
[20] Esfahani JA, Akbarzadeh M, Rashidi S, Rosen MA, Ellahi R. Influences of wavy wall and nanoparticles on entropy generation in a plate heat exchanger. Int J Heat Mass Transfer 2017;109:1162–71.
[21] Rashidi S, Esfahani JA, Ellahi R. Convective heat transfer and particle motion in an obstructed duct with two side-by-side obstacles by means of DPM model. Appl Sci 2017;7:431.
[22] Hayat T, Ullah I, Muhammad T, Alsaedi A. Thermal and solutal stratification in mixed convection three-dimensional flow of an Oldroyd-B nanofluid. Results Phys 2017;7:3797–805.
[23] Hayat T, Ullah I, Alsaedi A, Waqas M, Ahmad B. Three-dimensional mixed convection flow of Sisko nanoliquid. Int J Mech Sci 2017;133:273–82.
[24] Hayat T, Sajjad R, Muhammad T, Alsaedi A, Ellahi R. On MHD nonlinear stretching flow of Powell-Eyring nanomaterial. Results Phys 2017;7:535–43.
[25] Bhatti MM, Zeeshan A, Ellahi R. Simultaneous effects of coagulation and variable magnetic field on peristaltically induced motion of Jeffrey nanofluid containing gyrotactic microorganism. Microvasc Res 2017;110:32–42.
[26] Hassan M, Zeeshan A, Majeed A, Ellahi R. Particle shape effects on ferrofuids flow and heat transfer under influence of low oscillating magnetic field. J Magn Magn Mater 2017;443:36–44.
[27] Hayat T, Bashir G, Waqas M, Alsaedi A. MHD flow of Jeffrey liquid due to a nonlinear radially stretched sheet in presence of Newtonian heating. Results Phys 2016;6:817–23.
[28] Hayat T, Ullah I, Muhammad T, Alsaedi A. A revised model for stretched flow of third grade fluid subject to magneto nanoparticles and convective condition. J Mol Liq 2017;230:608–15.
[29] Hayat T, Ullah I, Ahmed B, Alsaedi A. MHD mixed convection flow of third grade liquid subject to non-linear thermal radiation and convective condition. Results Phys 2017;7:2804–11.
[30] Crane LJ. Flow past a stretching plate. Z Angew Math Phys 1970;21:645–7.
[31] Grubka LG, Bobba KM. Heat transfer characteristics of a continuous stretching surface with variable temperature. ASME J Heat Transfer 1985;107:248–50.
[32] Hayat T, Khan MI, Waqas M, Alsaedi A. Stagnation point flow of hyperbolic tangent fluid with Soret-Dufour effects. Results Phys 2017;7:2711–7.
[33] Waqas M, Khan MI, Hayat T, Alsaedi A. Stratified flow of an Oldroyd-B nanoliquid with heat generation. Results Phys 2017;7:2489–96.
[34] Hayat T, Khan MI, Waqas M, Alsaedi A. On Cattaneo-Christov heat flux in the flow of variable thermal conductivity Eyring-Powell fluid. Results Phys 2017;7:446–50.
[35] Hayat T, Zubair M, Waqas M, Alsaedi A, Ayub M. On doubly stratified chemically reactive flow of Powell-Eyring liquid subject to non-Fourier heat flux theory. Results Phys 2017;7:99–106.
[36] Hayat T, Khan MI, Waqas M, Alsaedi A. Newtonian heating effect in nanofluid flow by a permeable cylinder. Results Phys 2017;7:256–62.
[37] Hayat T, Ullah I, Alsaedi A, Ahmad B. Radiative flow of Carreau liquid in presence of Newtonian heating and chemical reaction. Results Phys 2017;7:715–22.
[38] Hayat T, Ullah I, Muhammad T, Alsaedi A, Shehzad SA. Three-dimensional flow of Powell-Eyring nanofluid with heat and mass flux boundary conditions. Chin Phys B 2016;25:074701.
[39] Mahapatra TR, Gupta AS. Magnetohydrodynamics stagnation-point flow towards a stretching sheet. Acta Mech 2001;152:191–6.
[40] Vajravelu K. Viscous flow over a nonlinearly stretching sheet. Appl Math Comput 2001;124:281–8.
[41] Cortell R. Effects of viscous dissipation and radiation on the thermal boundary layer over a nonlinearlystretching sheet. Phys Lett A 2008;372:631–6.
[42] Hayat T, Hussain Q, Javed T. The modified decomposition method and Padé approximants for theMHD flow over a non-linear stretching sheet. Nonlinear Anal: Real World Appl 2009;10:966–73.
[43] Rana P, Bhargava R. Flow and heat transfer of a nanofluid over a nonline4arly stretching sheet: a numerical study. Commun Nonlinear Sci Numer Simul 2012;17:212–26.
[44] Mukhopadhyay S. Analysis of boundary layer flow over a porous nonlinearly stretching sheet with partial slip at the boundary. Alex Eng J 2013;52:563–9.
[45] Mabood F, Khan WA, Ismail AIM. MHD boundary layer flow and heat transfer of nanofluids over a nonlinear stretching sheet: a numerical study. J Magn Magn Mater 2015;374:569–76.

[46] Mustafa M, Khan JA, Hayat T, Alsaedi A. Analytical and numerical solutions for axisymmetric flow of nanofluid due to non-linearly stretching sheet. Int J Non-Linear Mech 2015;71:22–9.
[47] Rashidi S, Dehghan M, Ellahi R, Riaz M, Jamal-Abad MT. Study of stream wise transverse magnetic fluid flow with heat transfer around an obstacle embedded in a porous medium. J Magn Magn Mater 2015;378:128–37.
[48] Hayat T, Ullah Ikram, Muhammad T, Alsaedi A. Magnetohydrodynamic (MHD) three dimensional flow of second grade nanofluid by convectively heated exponentially stretching surface. J Mol Liq 2016:1004–10120.
[49] Liao SJ. Homotopy analysis method in nonlinear differential equations. Heidelberg: Springer & Higher Education Press; 2012.
[50] Hayat T, Ullah I, Alsaedi A, Ahmad B. Modeling tangent hyperbolic nanoliquid flow with heat and mass flux conditions. Eur Phys J Plus 2017;132:112.
[51] Hayat T, Ullah I, Muhammad T, Alsaedi A. Radiative three-dimensional flow with Soret and Dufour effects. Int J Mech Sci 2017. https://doi.org/10.1016/j.ijmecsci.2017.09.015.
[52] Waqas M, Farooq M, Khan MI, Alsaedi A, Yasmeen T. Magnetohydrodynamic (MHD) mixed convection flow of micropolar liquid due to nonlinear stretched sheet with convective condition. Int J Heat Mass Transfer 2016;102:766–72.
[53] Hayat T, Khan MI, Farooq M, Alsaedi A, Yasmeen T. Impact of Cattaneo-Christov heat flux model in flow of variable thermal conductivity fluid over a variable thicked surface. Int J Heat Mass Transfer 2016;99:702–10.
[54] Waqas M, Hayat T, Farooq M, Shehzad SA, Alsaedi A. Cattaneo-Christov heat flux model for flow of variable thermal conductivity generalized Burgers fluid. J Mol Liq 2016;220:642–8.
[55] Waqas M, Alsaedi A, Shehzad SA, Hayat T, Asghar S. Mixed convective stagnation point flow of Carreau fluid with variable properties. J Braz Soc Mech Sci Eng 2017;39:3005–17.
[56] Waqas M, Khan MI, Hayat T, Alsaedi A, Khan MI. On Cattaneo-Christov double diffusion impact for temperature-dependent conductivity of Powell-Eyring liquid. Chin J Phys 2017;55:729–37.
[57] Makinde OD, Khan WA, Khan ZH. Buoyancy effects on MHD stagnation point flow and heat transfer of a nanofluid past a convectively heated stretching/shrinking sheet. Int J Heat Mass Transfer 2013;62:526–33.
[58] Hayat T, Ullah I, Alsaedi A, Farooq M. MHD flow of Powell-Eyring nanofluid over a non-linear stretching sheet with variable thickness. Results Phys 2017;7:189–96.